JOURNAL OF SOLID STATE CHEMISTRY 61, 369–378 (1986)

Order–Disorder in $CuIn_5Te_8$

N. FRANGIS,* G. VAN TENDELOO, J. VAN LANDUYT, AND S. AMELINCKX†

University of Antwerp (RUCA) Groenenborgerlaan 171; B-2020 Antwerp, Belgium

Received May 3, 1985; in revised form July 22, 1985

High-resolution electron microscopic observations show that $CuIn_5Te_8$ exhibits a somewhat disordered thiogallate structure. The domain structure, which is due to different arrangements of the cations within a common face centered cubic tellurium sublattice, is consistent with the symmetry of the thiogallate structure. After rapid cooling the crystals show short-range order. Within the face-centered cubic tellurium sublattice tetrahedral clusters consisting of three cations and one vacancy are the predominant species. © 1986 Academic Press, Inc.

1. Introduction

Among the ternary compounds of the chalcopyrite, thiogallate and defect stannite type a number is of potential interest as materials for photovoltaic solar energy conversion devices, since the bandgap of some of them is well adapted to the solar spectrum. The use of these compounds may nevertheless be hampered by the presence of structural defects. It is therefore of importance to study the microtexture of these compounds as well as the order–disorder phenomena.

In previous papers a number of these compounds was studied using mainly diffraction contrast. In the compound $CdIn_2Se_4$ three different phases with, respectively, $c = a$, $2a$, and $4a$ were identified (*1*). The domain structure of the compound $CuIn_5Se_8$ was described in Ref. (*2*) and two differently ordered spinel structures were found in $CuIn_5S_8$ (*3*, *4*). The compound $AgIn_5Se_8$ was studied in Ref. (*5*). In the present paper we shall limit ourselves to the compound $CuIn_5Te_8$, of which the domain structure was already discussed in Ref. (*6*) making use of diffraction contrast only. It was suggested on the basis of indirect evidence, derived from the domain structure, that this compound has the thiogallate structure, but no definite choice could be made between the defect stannite and the thiogallate structures, which differ only in the occupation of some of the tetrahedral interstices.

It is the purpose of this paper to describe some complementary observations with the high-resolution electron microscopy and to propose an interpretation for the diffuse scattering occurring in this compound and which is probably characteristic for several compounds of this family.

* On leave from: University of Thessaloniki, Thessaloniki, Greece.

† Also at SCK/CEN, B 2400-MOL.

0022-4596/86 $3.00

2. Structural Considerations

The compound $CuIn_5Te_8$ has either the thiogallate or the defect stannite structure which are both tetragonal with lattice parameters $a = 0.615$ nm and $c = 1.232$ nm (*6, 7*). The thiogallate structure is represented in Fig. 1a. Interchanging the atoms labeled 1 and 2 and their homologs produces the defect stannite structure. Both noncentrosymmetric structures can be considered as ordered derivatives of the sphalerite structure. The tellurium sublattice is face-centered cubic, the tetrahedral interstices of one type in the tellurium sublattice are occupied by either copper or indium ions leaving still one-fourth of this family of tetrahedral interstices vacant; they have to be considered as structural vacancies. The second family of tetrahedral interstices is completely empty in the idealized structure. The compound can thus be described as a quarternary compound $CuIn_5\ Ti_8$, the vacancies being one of the constituents. The existence of the structural vacancies explains why the cation sublattice becomes disordered well below the melting point.

A priori one might expect that in different parts of the crystal different sets of tetrahedral interstices may be occupied, the resulting two structures are then related by an inversion operation.

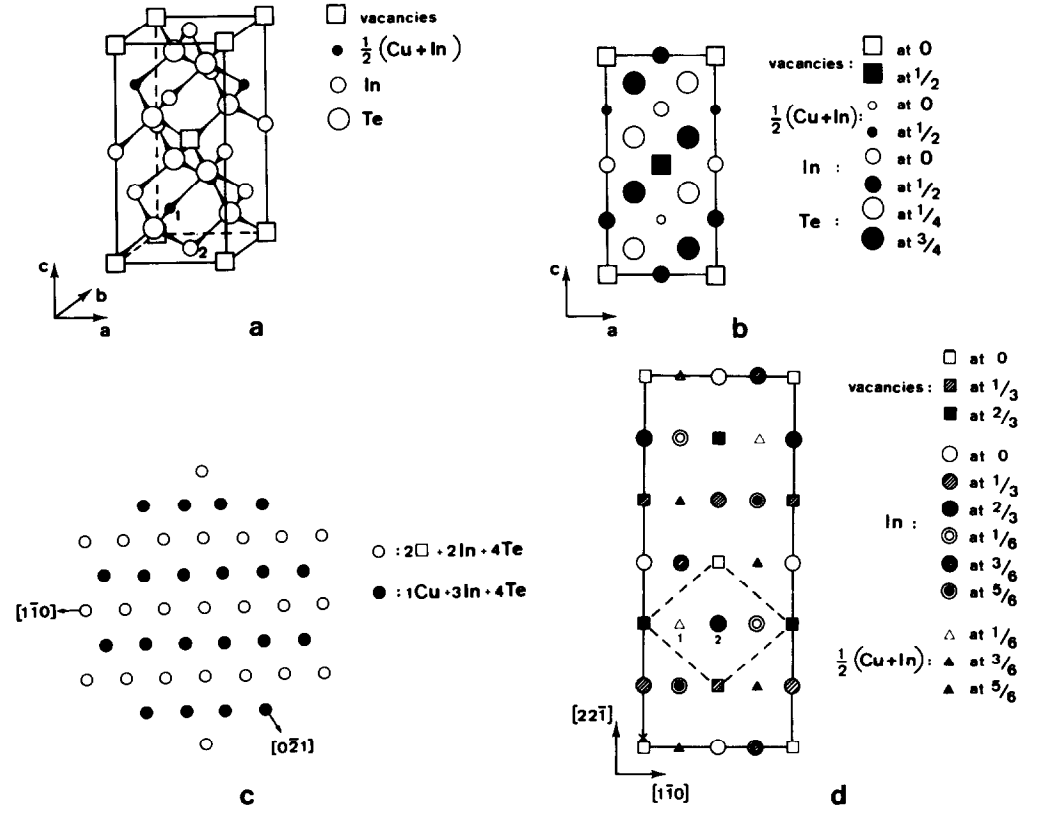

FIG. 1. Perspective drawing of the thiogallate-type structure ($CuIn_5Te_8$). (a) Spatial view of the structure. Interchanging the atoms at the sites 1 and 2, as well as on those at homologeous sites, produces the defect stannite structure. (b) Projection of the structure along the [010] zone. (b) Projection along the [221] direction. (d) [111] Zone view of the structure; all columns also contain tellurium in a slightly displaced position, which cannot be resolved.

Different projected views of the structure are also presented in Fig. 1. Figure 1b shows the projection along the [010] zone; the tellurium tetrahedra are not projected as squares.

Along the [221] zone (Fig. 1c) one can distinguish two kinds of columns: one type contains vacancies (one in four sites), the other one does not. They are situated in rows parallel with the [1$\bar{1}$0] direction and the two kinds of rows alternate. Both these projections are identical for the thiogallate and for the defect stannite structure and thus they do not allow to distinguish between the two possible structures.

The third projection, along [111] (in Fig. 1d), on the other hand, allows in principle to distinguish between the two structures provided one can see the difference between a column containing a mixture of copper and indium (such as 1 in Fig. 1d) and a column containing exclusively indium (such as 2 in Fig. 1d). The columns 1 and 2 are interchanged in the defect stannite structure. As a result of this one expects an asymmetrical arrangement of columns about the center of the long diagonal of the lozenge indicated by dotted lines in Fig. 1d. In the case of the defect stannite structure this arrangement would be symmetrical with respect to the center of the long diagonal. Since dot intensities at single-atom columns may randomly fluctuate somewhat it is more reliable to look along rows of columns averaging in this way the dot intensities.

Looking at grazing incidence along the rows of atom column parallel with the sides of the dotted lozenge one thus expects a sequence of rows containing in succession columns of vacancies, half indium and half copper, indium, indium, and vacancies again, etc. in the thiogallate structure. On the other hand, in the defect stannite structure one expects a sequence of rows containing successively columns of vacancies, indium, half copper and half indium, and again vacancies, etc. We shall see below that the high-resolution images allow to distinguish between these two possibilities.

3. Orientation Variants

The number of different orientation variants of the thiogallate structure can be derived in various ways. In (*2*) it was shown that with respect to the basic fcc anion sublattice the thiogallate structure (point group $\bar{4}$) can be formed in 12 ways. The sphalerite structure (point group $\bar{4}3m$) can be formed in two ways within the same anion sublattice, the two variants differing by an inversion operation. Within one of the sphalerite variants the thiogallate structure can be formed in 6 ways and the defect stannite structure (point group $\bar{4}2m$) in 3 ways (*6*). In principle the number of variants could allow to decide whether the structure is of the thiogallate type or of the defect stannite type. In practice this is not straightforward and the conclusion of Ref. (*6*) therefore remains somewhat ambiguous.

4. High-Resolution Images

High-resolution images were obtained along various simple zone axes, with a 200-kV electron microscope having a point resolution of about 0.25 nm. Figures 2a,b shows images made, respectively, along the [010] and the [221] zones. The corresponding diffraction patterns are reproduced in Figs. 3a and b. The bright-field images are made by including in the objective aperture the intense fcc reflections of the tellurium sublattice.

4.1. The [221] Zone (Fig. 2b)

The [221] zone corresponds with the [111] zone of the sphalerite structure; along this viewing direction the atom columns all have mixed composition. All columns contain tellurium but since along this zone the tetrahedral interstices project at the tellu-

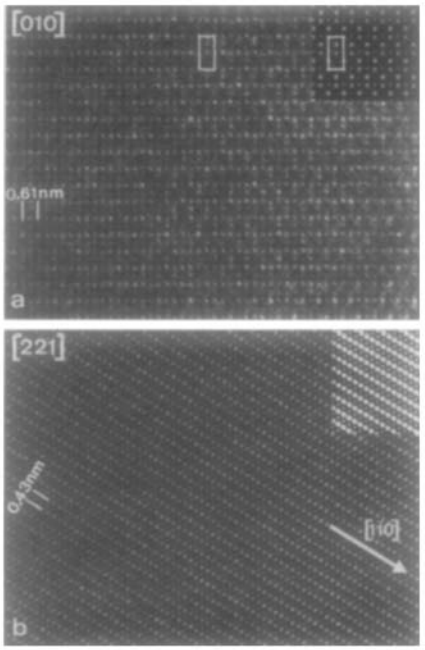

FIG. 2. High-resolution image of the $CuIn_5Te_8$ structure as viewed along [010] in (a) and along [221] in (b). The insets are computed images along the same zones.

rium positions all atom columns contain, next to tellurium, also either indium and vacancies or indium and copper. One can thus distinguish two types of columns of which the projections have been indicated by means of a different symbol in Fig. 1a. Similar atom columns project in close-packed rows parallel with the [1$\bar{1}$0] directions. The image of Fig. 2b clearly demonstrates the occurrence of the two kinds of [1$\bar{1}$0] rows of dots. The geometry and scale of the configuration of the brightest dots corresponds with the configuration of vacancy containing columns. In between the rows of brightest dots, rows of weaker bright dots are visible. In the calculated image, shown as an inset in Fig. 2b it was assumed that a vacancy-containing column occupied the origin; it exhibits the same features and allows to conclude that the vacancy-containing columns show up as the brightest dots.

4.2. *The [010] Zone (Fig. 2a)*

Along the [010] direction the structure is a column structure in the sense defined in Ref. (*8*), however certain columns contain indium as well as copper. The configuration and scale of the vacancy columns and that of the mixed columns is the same. The configuration of pure indium columns and of tellurium columns are different and also differ from that of the vacancy columns. The configuration of bright dots in Fig. 2a is the same as that of the pure-indium columns in Fig. 1b; they occur in pairs as do the bright dots in Fig. 2a and in the image simulation shown as inset (corresponding with Fig. 4 (e.g., $\Delta f = -60$ nm, $t = 14.7$ nm).

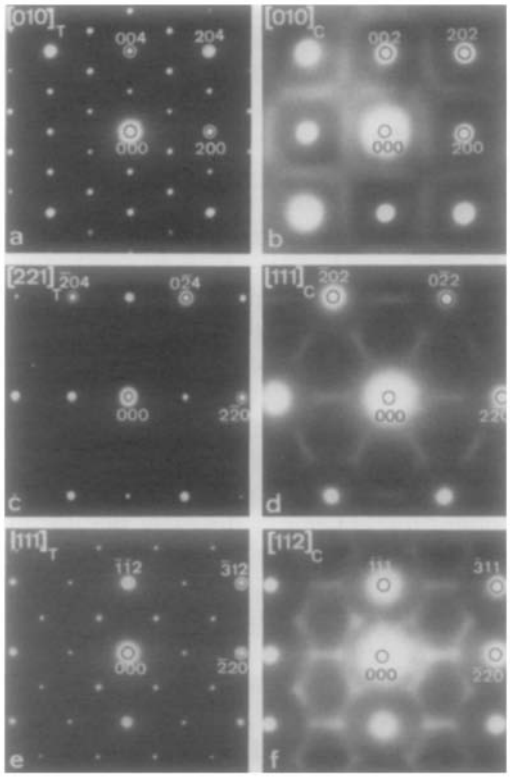

FIG. 3. Electron diffraction patterns of the long-range ordered (left) and short-range ordered (right) structures along three different zones: (a) and (b) [010] zone, (c) and (d) [221] zone, (e) and (f) [111] zone (tetragonal indices).

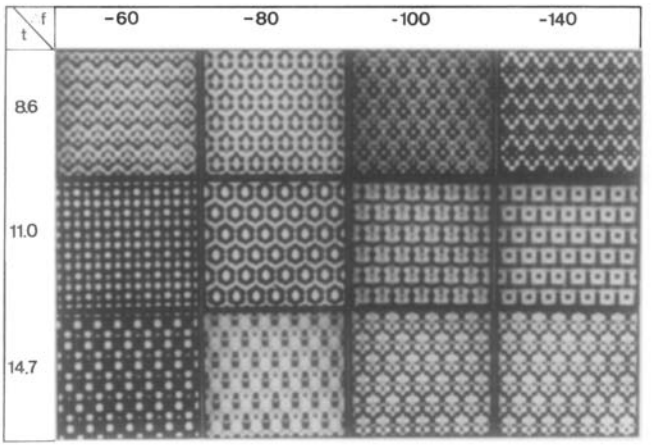

FIG. 4. Matrix of simulated images for different thicknesses (t) and defocus values (Δf). The structure is viewed along the [010] zone. A vacancy column was placed in the lower left corner.

However, the correspondence between the structure and the image is not as straightforward as these intuitive considerations would suggest. The matrix of images of Fig. 4 was computed for the model shown in Fig. 1a, i.e., with a vacancy column in the lower left corner. The brighter dots in the images obtained for $\Delta f = -60$ nm and $t = 11$ or 14.7 nm must then represent vacancy columns. Under these imaging conditions all bright dots represent either cation or vacancy columns, the tellurium columns being in the dark regions.

In the image with $\Delta f = -60$ nm and $t = 8.6$ nm on the contrary the largest dark dots come at positions of the Te columns, whereas smaller dark dots represent vacancy columns, and still smaller and weaker dark dots represent Cu + In columns, the indium columns being in the bright parts of the image.

4.3. *The [111] Zone*

The images along the [111] zone are represented in Figs. 5 to 10. All atom columns present are clearly resolved and imaged as dots of different brightness. The configuration of brightest dots is rectangular; alternatively it can be described as forming a centered lozenge (Fig. 1d).

The configuration of these brightest dots is the same as that of the vacancy columns and also as that of the columns containing half copper and half indium. Only image calculations allow to discriminate between the two possibilities; this is done further below.

The long diagonal of the lozenge (Fig. 1d) is divided into four equal parts by three atom columns. In the thiogallate structure

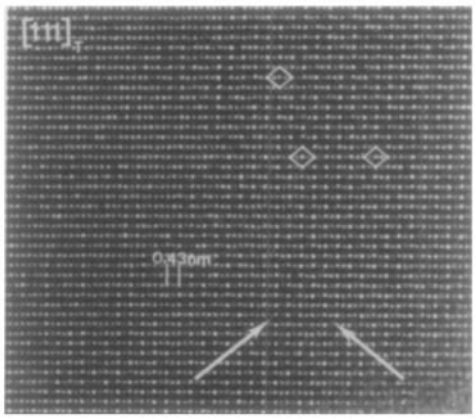

FIG. 5. High-resolution image of thiogallate structure along $[111]_T$.

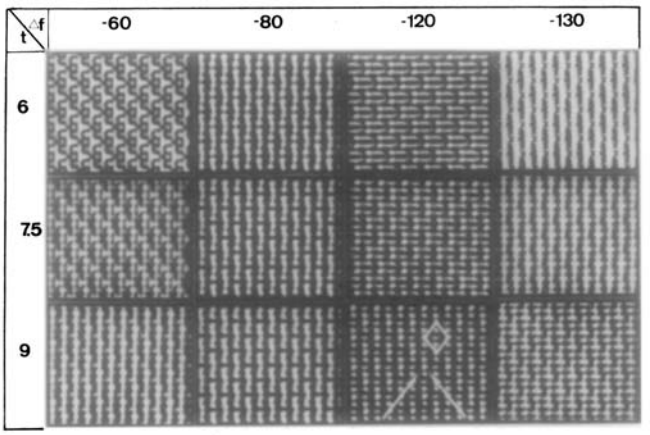

FIG. 6. Matrix of simulated images of the thiogallate structure along the [111] zone for different thicknesses (t) and defocus values (Δf). Looking at grazing incidence along the sides of the lozenge-shaped configurations the successive dot rows form an asymmetrical sequence.

these three columns have a different composition and one would thus expect them to show up with a different brightness. In fact they do so but not in the whole area of Fig. 5. Looking at grazing incidence along the sides of the lozenges, i.e., along the directions indicated by arrows one notes that every fourth dot row is darker than the other three. This means that systematically one of the three dots along the long diagonal is much weaker than the other two. This remark is independent of the fact whether the extra bright dots are interpreted as vacancy or as mixed columns. This observation is consistent with the thiogallate structure.

Looking along the [22$\bar{1}$] direction, i.e., parallel with the short diagonal of the lozenge one notes an alternation of bright and less bright rows of dots. This corresponds with the alternation of rows containing vacancy columns and those that do not.

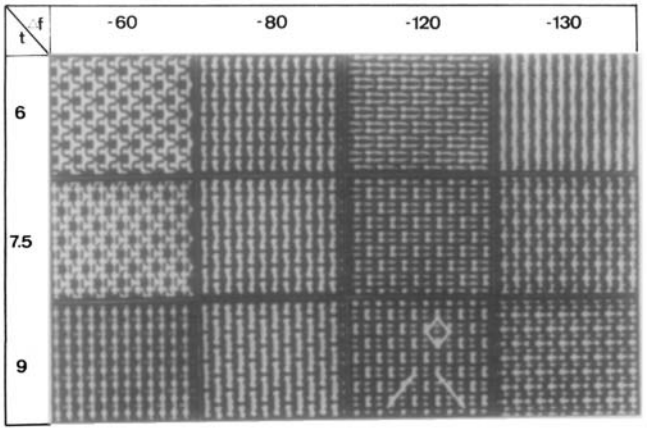

FIG. 7. Matrix of simulated images of the defect stannite structure along the [111] zone, for different thicknesses (t) and defocus value (Δf). Looking under grazing incidence along the sides of the lozenge-shaped arrangement of dots the intersections of the successive dot rows form a symmetrical sequence.

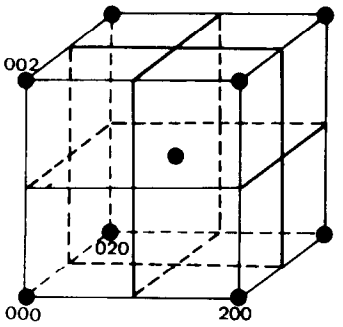

FIG. 8. Schematic representation of the lines of diffuse scattering in reciprocal space as observed in Fig. 3.

On the other hand, looking along the direction parallel with the long diagonal all dot rows look equally bright.

All these characteristics are absent in the region marked II in Fig. 10; in this part of the image there are no systematic brightness differences between rows of dots. Although the lattice of dots is continuous across the boundary there is thus a striking difference in the images as a result of differences in dot brightness. However, when looking at individual dots within different lozenges of extra bright dots one can find along the long diagonal "symmetrical" configurations suggesting the defect stannite structure, as well as "asymmetrical" ones characteristic of the thiogallate structure. This is also the case in Fig. 5.

The striking and abrupt difference in image characteristics between regions I and II in Fig. 10 is also evident from the optical diffraction patterns taken from these regions; whereas the superstructure is clearly revealed in region I, this is not the case in region II. This behavior can consistently be explained by assuming the presence of two different orientation variants in regions I and II. This interpretation is substantiated by the fact that the change in image contrast is abrupt along a well defined boundary; image changes as a result of thickness changes can be excluded from the sample geometry.

In region I the zone axis is $[111]_t$ with reference to the tetragonal axis or $[112]_c$ with reference to the cubic axis. In region II, on the other hand, we are looking along the $[241]_t$ zone, which is also the $[121]_c$ zone. The two variants are thus built on the same sphalerite sublattice since the $[112]_c$

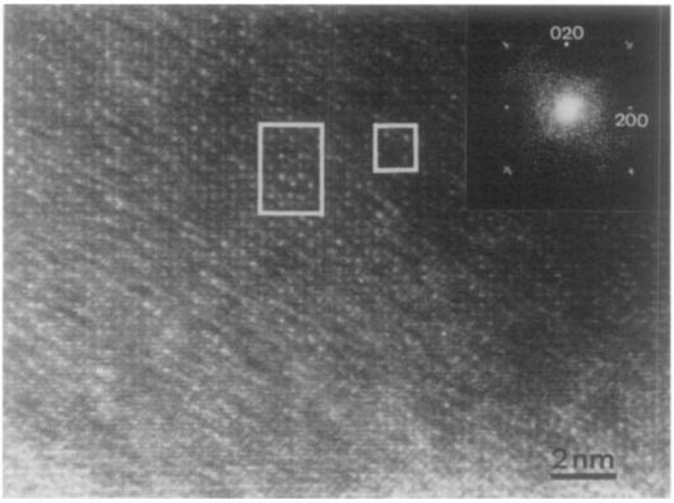

FIG. 9. High-resolution images of short-range ordered regions along the [010] zone. The inset shows the optical diffraction pattern exhibiting diffuse scattering.

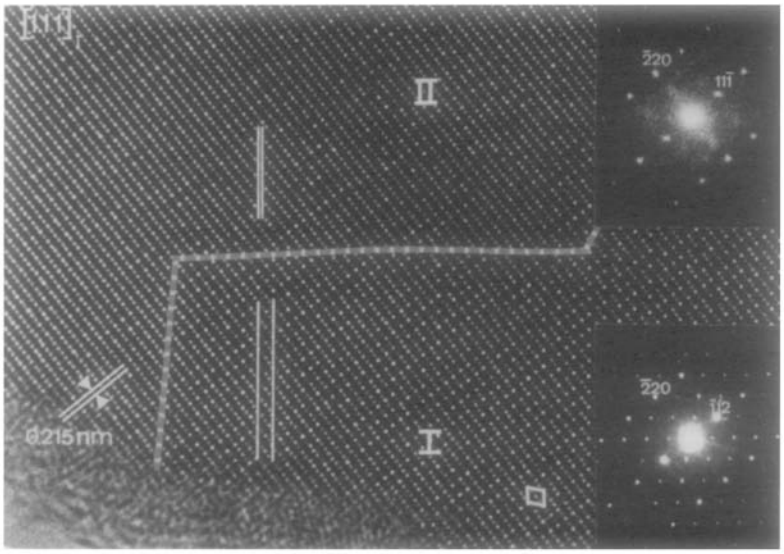

FIG. 10. High-resolution image of area of thiogallate structure containing two different orientation variants. Region I is viewed along $[111]_t$ zone whereas region II is viewed along the $[241]_t$ zone. The insets are optical diffraction patterns of these two regions.

and the $[121]_c$ directions are related by a symmetry operation of the cubic structure. This symmetry operation of the sphalerite structure is *not* a symmetry operation of the defect chalcopyrite or stannite structures and thus relates *two* different orientation variants. Along the $[111]_t$ zone the columns within a lozenge all contain in part tellurium, which projects very approximately along the same column, but are further different in composition; they thus show up with different brightnesses. This is not the case for the $[241]_t$ zone; along this zone all atom columns have the same composition in the ideal structure, equal to the macroscopic one, and they should thus all appear with the same brightness.

The described features are indeed observed in Fig. 10. In region I we find that statistically, i.e., by looking along the row of columns parallel to the white lines, the brightness of the three columns along the long diagonal of the lozenge are in agreement with the expectations for the thiogallate structure. However, this is only statistically true since it is derived from the relative brightness of dot rows. It should also be mentioned that when looking at individual dots in lozenges one finds "symmetrical" as well "asymmetrical" configurations (Fig. 5) suggesting some disorder along the atom columns.

In region II, on the other hand all, atom columns are statistically imaged as dot rows of equal brightness. Some disorder in the occupation of the columns is nevertheless again present, because locally some extra brighter or darker dots can be observed.

The differences in brightness are thought to reflect genuine differences in column composition since such differences occur apparently at random within regions of uniform contrast conditions. Under such conditions the only obvious reason for a difference in brightness seems to be the differences in composition. In alloys such

brightness differences between dots have also been attributed to composition differences (*9*).[1]

We conclude from this discussion that it is quite well possible that the defect thiogallate as well as the defect stannite structures may occur locally, intimately mixed.

5. Short-Range Ordered Structure

It is possible to obtain a disordered form of $CuIn_5Te_8$ either by quenching specimens from the growth temperature (667°C) or by beam heating in the microscope followed by rapid turning down of the beam current. The diffraction pattern along different zones of specimens treated in this way are reproduced in Figs. 3b,d, and f. The fcc reflections which are related to the tellurium sublattice, remain sharp. It is thus reasonable to attribute the diffuse scattering to disorder in the cation sublattice within an unperturbed fcc sublattice of tellurium atoms.

From the geometry of the regions of diffuse scattering one can deduce a so-called "cluster relation" in a binary system using the theory of Ref. (*10*). In reality the system has to be considered as a ternary consisting of Cu, In, and vacancies. However, it is not unreasonable to assume that at high-temperature copper and indium will behave rather similarly and in particular will become both mobile, be it at somewhat different temperatures. Close to the melting point, from where the specimens are quenched, it is thus possible to consider the system to a first approximation as a binary system consisting of cations and structural vacancies in the ratio 3 : 1. The pattern of diffuse scattering consists of lines parallel to the three cubic directions (Fig. 3b), they can be approximated by the equation $h = 2n + 1$; $k = 2n$ (or $l = 2n$) and all permutations.

It was shown in Ref. (*10*) that the corresponding cluster relation requires that the sites of a tetrahedral cluster should be occupied by the constituents in their macroscopic proportions, i.e., by three cations and one vacancy. This is clearly the case in the structure as represented in Fig. 1a; and it remains the case after interchanging the atoms 1 and 2. The cluster relation is thus satisfied in the thiogallate as well as in the defect stannite structures. When introducing antiphase boundaries on (001) planes with a displacement vector $\frac{1}{2}[110]$ the cluster relation is still satisfied across the antiphase boundary.

A plausible form of disorder, which would be consistent with the observed diffuse scattering, presents the following features. The basic framework of tellurium atoms remains unperturbed. The superstructure is present with equal probability with its *c*-axis along the three cube directions. Each of the orientation variants could moreover be fragmented by randomly distributed antiphase boundaries on cube planes. In this way the cluster relation would be satisfied everywhere, except perhaps along intersection lines of antiphase boundaries.

The segments of diffuse scattering consist of long streaks covering the spot positions corresponding with the superstructure reflections due to the different variants of the 2c and 4c polytypes. The segments end at some distance from the basic spots showing that the separation of the antiphase boundaries is rather uniformly distributed within a limited range so as *not* to give rise to pseudoperiods contributing to the intensity at the positions of higher order reflections.

This type of disorder turns out to be rather similar to that occurring in the alloy Pt_3V as described in Ref. (*11*). In the latter

[1] In a forthcoming paper the effect of overall composition and of the positioning of atoms of different chemical species along the column will be examined in more detail.

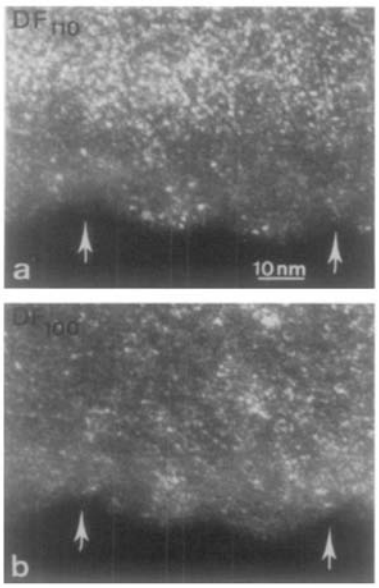

FIG. 11. Dark-field images of a short-range ordered specimen taken in the diffuse scattering of Fig. 3b. (a) Aperture is centered around the 101 position; (b) aperture is centered around the 100 position.

case simulation experiments on optical masks lead to the observed diffuse scattering patterns.

We have also attempted to obtain high-resolution images of quenched specimens. The image quality was not as good as for well-ordered specimens but nevertheless some conclusions could be drawn. From Fig. 9 which is a [001] view, it is evident that locally some configurations of bright dots occur, which can be compared with the image of Fig. 2a, suggesting that small ordered regions might still be present. Since according to the proposed model antiphase boundaries would also be present in planes parallel with the foil plane, one would not expect to see well-differentiated atom columns, except by chance and at most in small areas.

Dark-field images were made by selecting parts of the diffuse streaks. Figures 11a and b are dark-field images of the same area but made in different parts of the diffuse streaks; (a) is made by centering the objective aperture at the 101 position and (b) at the 100 position. The bright spots represent areas which contribute to the intensity in the chosen position. These images suggest that the specimens should contain small ordered domains, which reflect at the positions of the long-range order spots (Fig. 11a). The two types of observations are consistent with the model, whereby it is assumed that the crystal is highly fragmented by antiphase boundaries leaving only small domains of ordered structure.

References

1. C. MANOLIKAS, D. BARTZOKAS, G. VAN TENDELOO, J. VAN LANDUYT, AND S. AMELINCKX, *Phys. Status Solidi A* **59,** 425 (1980).
2. C. MANOLIKAS, J. VAN LANDUYT, R. DE RIDDER, AND S. AMELINCKX, *Phys. Status Solidi A* **55,** 709 (1979).
3. C. MANOLIKAS, R. DE RIDDER, J. VAN LANDUYT, AND S. AMELINCKX, *Phys. Status Solidi A* **59,** 621 (1980).
4. C. PAORICHI AND L. ZANOTTI, *Mater. Res. Bull.* **14,** 469 (1979).
5. N. FRANGIS, G. VAN TENDELOO, C. MANOLIKAS, J. SPYRIDELIS, J. VAN LANDUYT, AND S. AMELINCKX, *J. Solid State Chem.* **58,** 301 (1985).
6. H. HAHN, G. FRANK, W. KLINGLEV, A. D. STORGER, AND G. STORGER, *Z. Anorg. Chem.* **279,** 241 (1955).
7. N. FRANGIS, C. MANOLIKAS, AND J. SPYRIDELIS, *Mater. Res. Bull.* **17,** 1089 (1982); M. ROBBINS AND M. A. MIKOVSKY, *Mater. Res. Bull.* **6,** 359 (1971).
8. G. VAN TENDELOO AND S. AMELINCKX, *Phys. Status Solidi A* **47,** 555 (1978).
9. N. KUWANO, S. SASAKI, Y. TOMOKIYO, AND T. EGUCHI, "Electron Microscopy 1982," Proc. Hamburg 1982, p. 43.
10. R. DE RIDDER, G. VAN TENDELOO, D. VAN DYCK, AND S. AMELINCKX, *Phys. Status Solidi A* **38,** 663 (1976); R. DE RIDDER, D. VAN DYCK, G. VAN TENDELOO, AND S. AMELINCKX, *Phys. Status Solidi A* **40,** 669 (1977); R. DE RIDDER, G. VAN TENDELOO, AND S. AMELINCKX, *Acta Crystallogr. Sect. A* **32,** 216 (1976).
11. D. SCHRYVERS, G. VAN TENDELOO, AND S. AMELINCKX, *Mater. Res. Bull.* **20,** 361 (1985).